Reducing Transient Active- and Reactive-power Coupling in Virtual Synchronous Generators

Shuan Dong and Yu Christine Chen
Department of Electrical and Computer Engineering
The University of British Columbia
Vancouver, BC, Canada
Email: shuan@ece.ubc.ca, chen@ece.ubc.ca

***Abstract*—The virtual synchronous generator is a controller that regulates both active- and reactive-power outputs from a power-electronic converter. In order to vary its output active-power response speed freely, recent research has augmented this controller with the damping correction loop or the transient droop function. By combining these, this paper presents a virtual synchronous generator design that reduces the coupling between its active- and reactive-power outputs while allowing the response speed to be tuned freely. We provide analytical justification for the active- and reactive-power coupling by studying the system transfer function. Closed-form expressions for parameter values are derived to facilitate controller tuning. Finally, we verify the effectiveness of the proposed design via numerical simulations.**

I. Introduction

Driven by the goal of environmentally sustainable development, converter-interfaced renewable energy sources (RESs), e.g., wind and solar, are expected to gradually displace conventional fossil fuel-based synchronous generators in the existing power grid. This paradigm shift reshapes power system dynamics and presents numerous challenges to reliable and efficient grid operations. For example, the future power system is expected to have reduced inertia with increasing penetration of RESs, and consequently, it is at greater risk for instability following power demand-supply imbalances. This is because RESs generally interconnect to the grid via power-electronic converters, particularly voltage source converters (VSCs), that do not contribute inertia. Also, conventional controllers of RES power-electronic converters rely on phase-locked loops (PLLs) for measurements of the grid-side voltage phase angle. However, as revealed in [1], the adoption of PLLs may cause instability, especially under weak-grid conditions. Furthermore, RES generation is intermittent and variable, which may lead to large deviations in the grid-voltage frequency and magnitude, and consequently, poor power quality.

In order to address the limitations above, the concept of the virtual synchronous generator (VSG) has received considerable attention (see, e.g., [2]–[15]). Unlike conventional controllers for the RES power-electronic interface, the VSG is able to provide so-called virtual inertia to the power grid by emulating a synchronous generator. Also, the VSG avoids PLL-related instabilities by removing it from the controller design. Furthermore, the VSG can achieve frequency- and voltage-droop control, and in so doing, help improve the power quality and grid stability. However, most existing VSG designs cannot adjust their response speed without affecting the frequency-droop control characteristics, and this hinders the widespread adoption of VSGs in RES integration.

To deal with the aforementioned issue, the so-called *damping correction loop* and *transient droop function* have been proposed for the VSG to adjust its response speed freely without affecting droop characteristics [4], [16]. However, one shortcoming in VSG designs augmented with either the damping correction loop *or* the transient droop function is that its active-power loop (APL) and reactive-power loop (RPL) are not completely decoupled. For example, adjusting the RPL regulation signal $Q_t^\star$ may not only affect the reactive-power output Q_t (as expected), but also cause transient variations in the VSG active-power output P_t, which is undesirable. Particularly, if the APL is tuned to respond quickly, the VSG augmented with the damping correction loop results in lower active- and reactive-power coupling (i.e., smaller transient overshoot in P_t) than transient droop function, and vice-versa for slow response speed. Transient active-power variations may then cause unwanted grid-voltage frequency deviations, consequently adversely affecting power quality. The output-power coupling may result from high line-resistance-to-reactance ratio or large phase-angle difference between the converter output voltage and the grid-side voltage. In this paper, we deal with the coupling caused by the large power angle, since existing methods, such as the coordinate transformation method [11], [17], the virtual negative resistor method [18], and the virtual impedance method [7], can reshape the grid impedance and reduce the associated output-power coupling. In order to reduce the APL-RPL coupling caused by large phase-angle difference, the cross feedforward compensation [9], the linear control theory-based approach [6], and the current compensation method [8] have been proposed. However, these either cannot freely adjust the VSG response speed, or they significantly complicate the controller structure.

The contributions of this paper are as follows. We propose to combine the damping correction loop and the transient droop function in order to reduce the coupling between the APL and RPL regardless of the tuned VSG response speed. The proposed combination reduces the impact of the RPL input on the APL output, which is more severe than that of the APL on the RPL. Moreover, since the original damping correction loop design in [4] may saturate the controller, we adopt a different realization of this loop that avoids saturation. Also, we provide analytical justification for the proposed design via transfer-function analysis. Closed-form expressions for parameter values are derived to facilitate controller tuning.

The remainder of this paper is organized as follows. In Section II, we describe the proposed controller design. Then, in Section III, we analyze the transfer function of the proposed design, study the output-power coupling, and derive parameter settings to achieve desired dynamic behaviour. Finally, in Section IV, we validate the effectiveness of the proposed controller via extensive simulations.

II. Proposed Controller Design

As shown in Fig. 1(c), the VSG controller, which is embedded within the VSC, is connected to the grid via filter R_s+jX_s and transmission line R_e+jX_e, with the assumption that $X_t = X_s + X_e \gg R_s + R_e$. In order to adjust the VSG response speed freely and simultaneously reduce the coupling between the APL and the RPL, we propose to add both the damping correction loop and the transient droop function into the APL, as depicted in Fig. 1(a). With these augmented, the dynamics for the VSG rotating speed ω_g can be expressed as

$$J_g \frac{d\omega_g}{dt} = T_m - T_{ef} - D_p(\omega_g - \omega_g^\star) - (T_1 + T_2), \quad (1)$$

where J_g is a tuneable inertia parameter, $T_m = P_t^\star/\omega_N$ is the input torque (with $P_t^\star$ as the reference value of active-power output P_t and ω_N as the rated value of ω_g), T_{ef} is the filtered electrical torque T_e, and $\omega_g^\star$ is the reference value of ω_g. In (1), the term $-D_p(\omega_g-\omega_g^\star)$ achieves frequency-droop control, with D_p being the droop constant and determined by $D_p = \Delta T_m/\Delta\omega_g$, where $\Delta\omega_g = \omega_g - \omega_g^\star$ denotes the angular speed deviation, and ΔT_m represents the amount of input torque change required by local grid code [4].

In order to present the core ideas behind T_1 and T_2, we neglect the low-pass filters (LPFs), marked as LPF1 and LPF2 in Fig. 1(a). (On the other hand, later in Section III-C, we will fully consider these LPFs for the purpose of parameter tuning [5].) Then, the outputs of the damping correction loop and the transient droop function are expressed as [4], [16]

$$T_1 \approx D_f \frac{d}{dt}\left(i_g^{\mathrm{T}} \sin\widetilde{\theta}_g\right), \quad T_2 \approx D_m \frac{dP_t}{dt}, \quad (2)$$

respectively, where D_f $[\mathrm{V}\cdot\mathrm{s}^2/\mathrm{rad}]$ and D_m $[\mathrm{s}^2/\mathrm{rad}]$ are tuneable parameters, $i_g = [i_{ga},\ i_{gb},\ i_{gc}]^{\mathrm{T}}$ is the output current, and $\sin\widetilde{\theta}_g = [\sin\theta_g,\ \sin(\theta_g - \frac{2\pi}{3}),\ \sin(\theta_g + \frac{2\pi}{3})]^{\mathrm{T}}$ (with θ_g denoting the rotor angle). In (2), the term T_1 represents a different realization of the damping correction loop from the one in [4], i.e., $D_f \frac{d}{dt}\left(\frac{T_{ef}}{\psi_{ff}}\right)$, where ψ_{ff} denotes the filtered excitation flux ψ_f obtained from the RPL. As we illustrate later, T_1 adjusts the APL response speed in the same way as the realization in [4], but avoids the potential shortcoming of saturating the controller when $\psi_{ff} = 0$. Let $\theta_{g\infty}$ denote the phase-angle difference between the inner voltage e_g and the grid voltage u_∞. Note that $e_g = \omega_g\psi_f\sin\widetilde{\theta}_g$ and $\omega_g \approx \omega_N$. Then, neglecting circuit (see Fig. 1(c)) dynamics in the time scales that we consider, the VSG active-power output P_t an can be expressed as

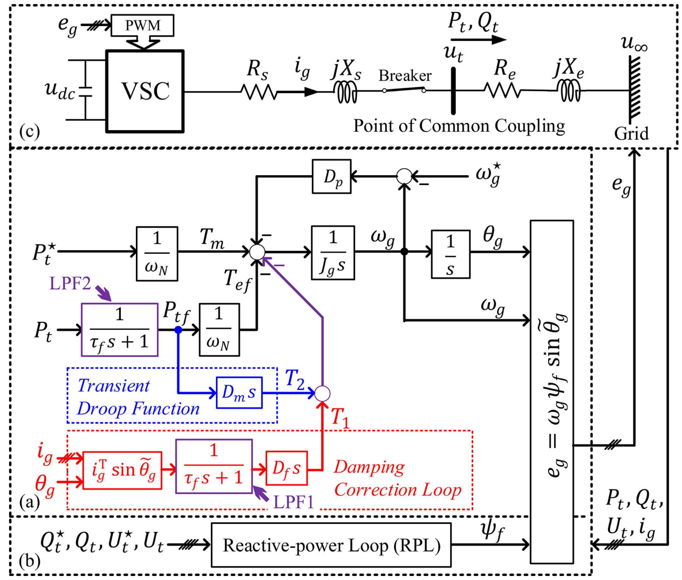

Fig. 1. Proposed VSG design that combines the damping correction loop and the transient droop function. Specifically, by setting $D_m = 0$, this figure represents the VSG with the damping correction loop only, and by setting $D_f = 0$, this figure represents the VSG with the transient droop function only). This controller design is able to reduce the coupling between active- and reactive-power loops regardless of the tuned VSG response speed.

$$P_t \approx i_g^{\mathrm{T}} e_g \approx \sqrt{\frac{3}{2}}\frac{\omega_N\psi_f U_\infty}{X_t}\sin\theta_{g\infty}, \quad (3)$$

and the term $i_g^{\mathrm{T}}\sin\widetilde{\theta}_g$ in (2) can be expressed as

$$i_g^{\mathrm{T}}\sin\widetilde{\theta}_g = i_g^{\mathrm{T}}\frac{e_g}{\omega_g\psi_f} \approx \frac{P_t}{\omega_N\psi_f} = \sqrt{\frac{3}{2}}\frac{U_\infty}{X_t}\sin\theta_{g\infty}, \quad (4)$$

where U_∞ is the line-to-line RMS value of u_∞. Then, by substituting (3) and (4) into (2), and further substituting $\frac{d\theta_{g\infty}}{dt} = \omega_g - \omega_\infty$ into the resultant, we get

$$T_1 = D_f\sqrt{\frac{3}{2}}\frac{U_\infty\cos\theta_{g\infty}}{X_t}(\omega_g - \omega_\infty), \quad (5)$$

$$T_2 = D_m\frac{\partial P_t}{\partial\theta_{g\infty}}(\omega_g - \omega_\infty) + D_m\frac{\partial P_t}{\partial\psi_f}\frac{d\psi_f}{dt}. \quad (6)$$

Based on expressions for T_1 and T_2 in (5) and (6), respectively, we make three key observations regarding the proposed design in Fig. 1. First, both T_1 and T_2 are zero at steady state, so neither affects the steady-state frequency-droop characteristics. Also, similar in form to $D_p(\omega_g-\omega_g^\star)$, both T_1 and T_2 provide tuneable damping torque components that adjust the APL response speed by varying APL damping. Finally, by omitting LPF1, T_1 in (5) is identical to $D_f\frac{d}{dt}\left(\frac{T_{ef}}{\psi_{ff}}\right)$ in [4], so blocks marked in red colour in Fig. 1(a) indeed represent another realization of the damping correction loop proposed in [4].

III. Transfer-function Analysis

In this section, we develop the transfer-function model for the APL in the proposed VSG design. Then by analyzing

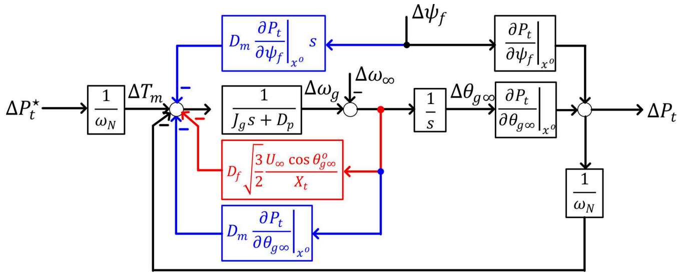

Fig. 2. Block diagram for small-signal model of the APL (omitting LPF1 and LPF2). The block marked in red is associated with the damping correction loop, and those in blue are related to the transient droop function.

the resulting model, we show that the proposed VSG design, which combines the damping correction loop and the transient droop function, reduces output-power coupling.

A. Transfer-function Model of the APL

To show that the inclusion of both the damping correction loop and the transient droop function with outputs T_1 and T_2, respectively, reduces coupling between the APL and RPL, we construct the small-signal model for the VSG APL in Fig. 1(a) by linearizing (1), (3), (5), and (6) around the equilibrium point (denoted by the superscript $\circ$) and taking the Laplace transformation of the resultant linear system. In this model, we consider small variations in the APL input variables $P_t^\star$, ω_∞, and ψ_f, denoted by $\Delta P_t^\star$, $\Delta\omega_\infty$, and $\Delta\psi_g$, respectively ($\omega_g^\star$ remains unchanged as it is a reference value). Further let $\Delta\theta_{g\infty}$ and ΔP_t denote the variations in $\theta_{g\infty}$ and P_t caused by the variations in the APL inputs. Then, as shown in Fig. 2, we get the following APL transfer-function model:

$$\Delta P_t = G_1(s)\Delta P_t^\star + G_2(s)\Delta\omega_\infty + G_3(s)\Delta\psi_f, \quad (7)$$

where

$$G_1(s) = \frac{\omega_n^2}{s^2+2\zeta\omega_n s+\omega_n^2}, \quad G_2(s) = \frac{-M(s+\alpha)}{s^2+2\zeta\omega_n s+\omega_n^2},$$
$$G_3(s) = \frac{N(s^2+\beta s)}{s^2+2\zeta\omega_n s+\omega_n^2}. \quad (8)$$

with coefficients M and N expressed as, respectively,

$$M = \sqrt{\frac{3}{2}}\frac{\omega_N\psi_f^\circ U_\infty\cos\theta_{g\infty}^\circ}{X_t}, \quad N = \sqrt{\frac{3}{2}}\frac{\omega_N U_\infty\sin\theta_{g\infty}^\circ}{X_t}.$$

In (8), the parameter $\alpha = D_p/J_g$; and further, damping ratio ζ, natural frequency ω_n, and parameter β are given by

$$\zeta = \frac{A}{\sqrt{J_g}}\left(D_p + \left(D_f + D_m\omega_N\psi_f^\circ\right)\sqrt{\frac{3}{2}}\frac{U_\infty\cos\theta_{g\infty}^\circ}{X_t}\right),$$
$$\omega_n = \frac{B}{\sqrt{J_g}}, \quad \beta = \frac{1}{J_g}\left(D_p + D_f\sqrt{\frac{3}{2}}\frac{U_\infty\cos\theta_{g\infty}^\circ}{X_t}\right), \quad (9)$$

respectively, where coefficients A and B satisfy, respectively,

$$A = \sqrt{\frac{\sqrt{6}X_t}{12\psi_f^\circ U_\infty\cos\theta_{g\infty}^\circ}}, \; B = \sqrt{\frac{\sqrt{6}\psi_f^\circ U_\infty\cos\theta_{g\infty}^\circ}{2X_t}}. \quad (10)$$

B. Analysis of Output-power Coupling

We focus our analysis on transfer function $G_3(s)$ in (8), as it represents the effect of the RPL output ψ_f on the APL output P_t, thus revealing the active- and reactive-power coupling. This coupling can be reduced by varying β in $G_3(s)$, which is linearly dependent on the tuneable parameter D_f and inversely proportional to J_g according to (9). To see the influence of β, decompose $G_3(s)$ as

$$G_3(s) = G_{31}(s) + G_{32}(s), \quad (11)$$

where

$$G_{31}(s) = \frac{Ns^2}{s^2+2\zeta\omega_n s+\omega_n^2}, \quad G_{32}(s) = \frac{N\beta s}{s^2+2\zeta\omega_n s+\omega_n^2}.$$

In the above, setting $\beta = 0$ eliminates the effect of $G_{32}(s)$ in $G_3(s)$. We recommend setting $\beta < 0$, since in so doing, $G_{32}(s)$ would further partially offset the effect of $G_{31}(s)$ in the resultant $G_3(s)$. In this way, we reduce the impact of the RPL output ψ_f on the APL output P_t dynamics. Additionally, the desired APL dynamic response can be achieved by setting ζ and ω_n to suitable values. As revealed in (9), the combination of the damping correction loop and the transient droop function provides three tuneable parameters J_g, D_f, and D_m, which give enough control freedom to set β, ζ, and ω_n to their desired values. Thus, the proposed VSG achieves both output-power decoupling and desired APL dynamic response speed. Such an outcome cannot be achieved with either the damping correction loop or the transient droop function alone, as in both of those cases, the APL has only two tuneable parameters J_g and D_f (or D_m). In fact, after tuning these two parameters for desired APL dynamic response, β is always positive, which causes greater APL and RPL coupling [4]. In Remark 1 below, we use the model in (7) to quantitatively compare the output-power coupling caused by the damping correction loop to that by the transient droop function in VSG.

Remark 1 (Comparison of Coupling in VSG Augmented with Damping Correction Loop vs. Transient Droop Function)**.** Let $\omega_n^\star$ and $\zeta^\star$, respectively, denote the desired APL natural frequency and damping ratio. We find that by setting $\omega_n^\star > \frac{B\zeta^\star}{AD_p}$ so that the APL responds quickly, the damping correction loop leads to less coupling; if $0 < \omega_n^\star < \frac{B\zeta^\star}{AD_p}$, the transient droop function results in less coupling; and if $\omega_n^\star = \frac{B\zeta^\star}{AD_p}$, the two designs have same output-power coupling. To see this, we first obtain the APL models of the two designs by setting, respectively, D_m and D_f to be zero in (7). Specifically, for the VSG augmented with only the damping correction loop, set $D_m = 0$ in (9), and we get

$$\zeta = \frac{A}{\sqrt{J_g}}\left(D_p + D_f\sqrt{\frac{3}{2}}\frac{U_\infty\cos\theta_{g\infty}^\circ}{X_t}\right) =: \zeta_{\mathrm{DCL}}, \quad (12)$$

$$\omega = \frac{B}{\sqrt{J_g}} =: \omega_{n,\mathrm{DCL}}, \quad (13)$$

$$\beta = \frac{1}{J_g}\left(D_p + D_f\sqrt{\frac{3}{2}}\frac{U_\infty\cos\theta_{g\infty}^\circ}{X_t}\right) =: \beta_{\mathrm{DCL}}. \quad (14)$$

On the other hand, for the VSG augmented with only the transient droop function, set $D_f = 0$ in (9) to get

$$\zeta = \frac{A}{\sqrt{J_g}}\left(D_p + D_m\omega_N\psi_f^\circ\sqrt{\frac{3}{2}}\frac{U_\infty\cos\theta_{g\infty}^\circ}{X_t}\right) =: \zeta_{\mathrm{TDF}}, \tag{15}$$

$$\omega = \frac{B}{\sqrt{J_g}} =: \omega_{n,\mathrm{TDF}}, \tag{16}$$

$$\beta = \frac{D_p}{J_g} =: \beta_{\mathrm{TDF}}. \tag{17}$$

Next, to ensure a fair comparison, via suitable choices for the values of J_g and D_f (or D_m), we set the damping ratios and natural frequencies of these two designs to the same reference values $\zeta^\star$ and $\omega_n^\star$, i.e.,

$$\zeta_{\mathrm{DCL}} = \zeta_{\mathrm{TDF}} = \zeta^\star, \quad \omega_{n,\mathrm{DCL}} = \omega_{n,\mathrm{TDF}} = \omega_n^\star. \tag{18}$$

Then, substituting J_g and D_f solved from (12) and (13) into (14), and J_g and D_m solved from (15) and (16) into (17), and taking the difference between the resultant expressions for β_{DCL} and β_{TDF}, we get

$$\beta_{\mathrm{DCL}} - \beta_{\mathrm{TDF}} = -\frac{D_p\omega_n^\star}{B^2}\left(\omega_n^\star - \frac{B\zeta^\star}{AD_p}\right). \tag{19}$$

Based on (19), if $\omega_n^\star > \frac{B\zeta^\star}{AD_p}$, then $\beta_{\mathrm{DCL}} - \beta_{\mathrm{TDF}} < 0$ and $\beta_{\mathrm{TDF}} > \beta_{\mathrm{DCL}} > 0$; if $0 < \omega_n^\star < \frac{B\zeta^\star}{AD_p}$, then $\beta_{\mathrm{DCL}} - \beta_{\mathrm{TDF}} > 0$ and $\beta_{\mathrm{DCL}} > \beta_{\mathrm{TDF}} > 0$; and if $\omega_n^\star = \frac{B\zeta^\star}{AD_p}$, then $\beta_{\mathrm{DCL}} - \beta_{\mathrm{TDF}} = 0$ and $\beta_{\mathrm{TDF}} = \beta_{\mathrm{DCL}} > 0$. Thus, with a larger value for $\omega_n^\star$, which ensures faster response speed, the VSG augmented with the damping correction loop has lower output-power coupling than that with the transient droop function. On the other hand, with a smaller value for $\omega_n^\star$, which achieves slower response speed, the VSG augmented with the damping correction loop has larger output-power coupling. Furthermore, if $\omega_n^\star = \frac{B\zeta^\star}{AD_p}$, the two methods result in identical APL and RPL coupling. ■

Via transfer-function analysis, we conclude that by combining the damping correction loop and the transient droop function, the proposed VSG design has reduced output-power coupling regardless of whether the APL response speed is tuned to be faster or slower. Next, we outline the parameter tuning procedure to achieve desired transient behaviour with respect to output-power coupling and response speed.

C. APL Parameter Tuning

Although the model developed in (7) is sufficiently accurate to reveal the effects of VSG active- and reactive-power coupling, it cannot be used directly to tune controller parameters [5]. This is because the filters LPF1 and LPF2 in Fig. 1(a) are neglected in (7) for ease of analysis. Thus, here, for purposes of parameter tuning, we fully include the effects of LPF1 and LPF2 to ensure accurate parameter values are chosen. To this end, denote by $\beta^\star$, $\zeta^\star$, and $\omega_n^\star$, the reference values for β, ζ, and ω_n to achieve desired output-power decoupling and APL response speed. Then, we obtain the following closed-form expressions for the APL parameters:

$$J_g = \frac{\sqrt{\frac{3}{2}}\psi_f^\circ U_\infty\cos\theta_{g\infty}^\circ - \tau_f D_p X_t {\omega_n^\star}^2}{{\omega_n^\star}^2 X_t(1 - 2\tau_f\omega_n^\star\zeta^\star)}, \tag{20}$$

$$D_f = \sqrt{\frac{2}{3}}\frac{X_t\left(\beta^\star J_g - D_p\right)}{U_\infty\cos\theta_{g\infty}^\circ}, \tag{21}$$

$$D_m = \frac{2\zeta^\star}{\omega_N\omega_n^\star} + \sqrt{\frac{2}{3}}\frac{J_g X_t({\omega_n^\star}^2\tau_f - \beta^\star)}{\omega_N\psi_f^\circ U_\infty\cos\theta_{g\infty}^\circ}. \tag{22}$$

Interested readers may refer to Appendix A for detailed derivation of (20)–(22).

TABLE I
PARAMETER VALUES USED TO VERIFY PROPOSED VSG DESIGN TUNED TO RESPOND QUICKLY (CASE I) AND SLOWLY (CASE II) IN SECTION IV-A1.

	Method	J_g (kg·m^2)	D_f (V·s/rad)	D_m (s/rad)
Case I	A	10	-6.0	6.7×10^{-4}
	B	10	-2.57	N/A
	C	10	N/A	-4.7×10^{-4}
Case II	A	803	-7.0	2.3×10^{-3}
	B	803	5.1	N/A
	C	803	N/A	9.6×10^{-4}

IV. SIMULATION VALIDATION

In this section, via numerical studies, we verify that the proposed VSG design indeed reduces its output-power coupling regardless of whether the APL is tuned to respond quickly or slowly. We also verify that the response speed of the proposed VSG can be tuned freely without affecting its steady-state frequency-droop characteristics. The simulated system as shown in Fig. 1 is modelled in PSCAD/EMTDC in conjunction with parameters as follows: $R_s + jX_s = 0.74 + j7.5\ \Omega$, $R_e + jX_e = 1.5 + j15\ \Omega$, $D_p = 1407\ \mathrm{N\cdot m\cdot s/rad}$, $\omega_N = \omega_g^\star = 377$ rad/s, and $U_\infty = 6.6$ kVrms.

A. Active- and Reactive-power Coupling

In this case study, we show that the proposed VSG design has lower output-power coupling than VSGs augmented with either the damping correction loop or the transient droop function alone. We also validate several analytical insights highlighted in Section III-B.

1) Reduced Coupling: We consider two cases in which the APL is tuned to respond (i) quickly (Case I: $\omega_n^\star = 15$ rad/s, $\zeta^\star = 0.8$, and $\beta^\star = -67$), and (ii) slowly (Case II: $\omega_n^\star = 2.5$ rad/s, $\zeta^\star = 0.8$, and $\beta^\star = -67$). The corresponding parameter values are reported in Table I. Note that parameters of the proposed design (method A) is computed according to (20)–(22), and satisfies $\omega_n^\star$, $\zeta^\star$, and $\beta^\star$ requirements, while using damping correction loop (method B) or transient droop function (method C) achieves only $\omega_n^\star$ and $\zeta^\star$ due to their limited control freedom. In Case I, as shown in Fig. 3(a), method A results in the least transient overshoot in P_t when $Q_t^\star$ increases from 0.0 to 0.4 MVar at $t = 4.0$ s compared with methods B and C. This is also observed in Fig. 3(b) for Case II, where the APL is tuned to respond slowly. Thus, indeed, the proposed VSG design effectively reduces the coupling between the APL

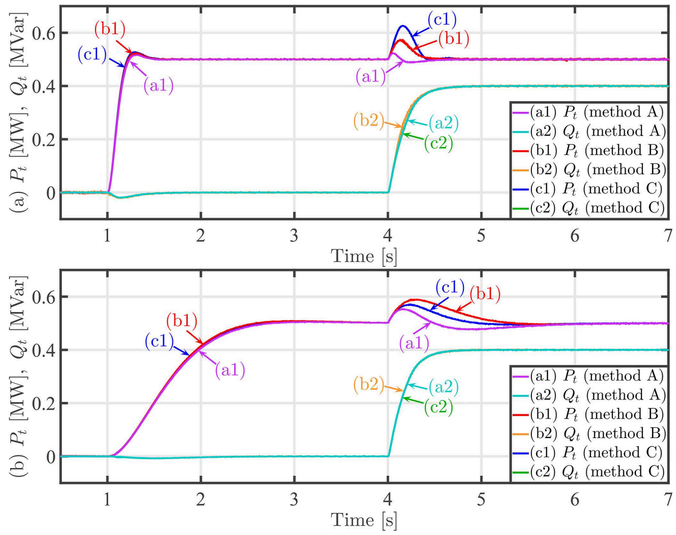

Fig. 3. Comparison of dynamic response of proposed VSG design (method A) with VSG augmented with only the damping correction loop (method B) and one with only the transient droop function (method C). Indeed, method A has the least coupling with (a) fast and (b) slow APL response speed.

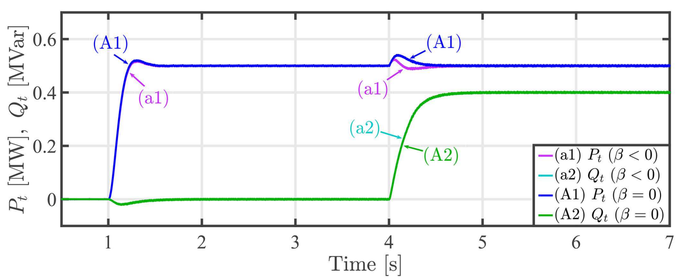

Fig. 4. Impact of β on active- and reactive-power coupling. By tuning parameters such that $\beta < 0$, active- and reactive-power coupling is reduced when compared with setting $\beta = 0$.

and the RPL, both when the APL is tuned to respond quickly and slowly. Moreover, following the step change in active-power reference $P_t^\star$ from 0.0 to 0.5 MW at $t = 1.0$ s, method A has identical dynamic response with methods B and C, effectively demonstrating that the response speed of the proposed design is fully adjustable. Moreover, these results validate the analytical expressions (20)–(22) that determine values of APL control parameters J_g, D_f, and D_m based on the desired transient behaviour.

2) Impact of β on Coupling: As stated in Section III-B, having $\beta < 0$ achieves better performance in reducing active- and reactive-power coupling. We verify this by comparing two cases, one with $\beta = -67 < 0$ and the other with $\beta = 0$. The controller is tuned to respond quickly, i.e, $\omega_n^\star = 15$ rad/s and $\zeta^\star = 0.8$. We note, however, that similar observations can be made when the VSG is tuned to respond slowly, and we refrain from further discussions thereof. As shown in Fig. 4, following the increase in Q_t from 0 to 0.4 MVar, the active power P_t in the case with $\beta < 0$ (trace (a1)) indeed has a smaller transient overshoot than that with $\beta = 0$ (trace A1).

3) Damping Correction Loop vs. Transient Droop Function: We verify the analysis presented in Remark 1 on the

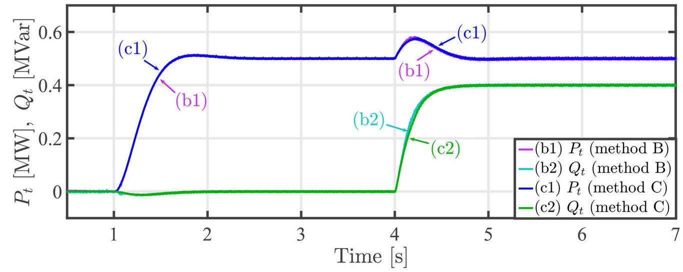

Fig. 5. Active- and reactive-power coupling in VSGs augmented with either damping correction loop (method B) or transient droop function (method C) are nearly identical with $\omega_n^\star = \frac{B\zeta^\star}{AD_p}$. Indeed, the relative values of $\omega_n^\star$ and $\frac{B\zeta^\star}{AD_p}$ determine whether the damping correction loop or the transient droop function results in lower coupling.

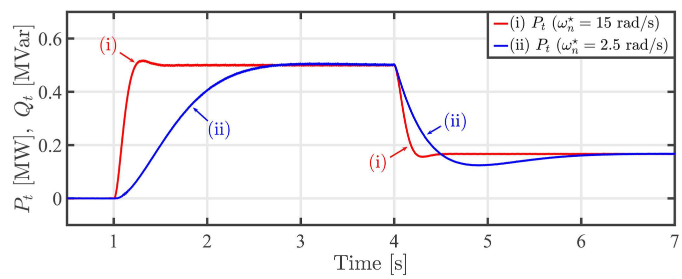

Fig. 6. Steady-state frequency-droop characteristics are maintained under both (i) fast and (ii) slow APL response speeds.

comparison between VSGs augmented with either the damping correction loop or the transient droop function. Here, set $\omega_n^\star = \frac{B\zeta^\star}{AD_p} = 5.6$ rad/s and consider a step change in the reactive-power reference value $Q_t^\star$ from 0 to 0.4 MVar at $t = 4.0$ s. As shown in Fig. 5, VSGs augmented with either the damping correction loop or the transient droop function have nearly identical active- and reactive-power coupling. Thus, $\frac{B\zeta^\star}{AD_p}$ is indeed the critical value for $\omega_n^\star$, and their relative values determine whether the damping correction loop or the transient droop function results in lower coupling.

B. Steady-state Frequency-droop Characteristics

In this case study, we validate that adjusting the APL response speed of the proposed VSG does not affect its steady-state frequency-droop characteristics. Suppose the grid frequency f_∞ drops from 60 to 59.9 Hz at $t = 4.0$ s. As depicted in Fig. 6, whether the VSG is tuned to respond quickly (trace (i)) or slowly (trace (ii)), the active power P_t converges to the same value at $t = 7.0$ s following the frequency step change at $t = 4.0$ s. The steady-state deviation is dictated by D_p, which is set to the same value $1407\ \mathrm{N\cdot m\cdot s/rad}$ for both scenarios of fast and slow response speed.

V. Concluding Remarks

In this paper, we propose to reduce the VSG active- and reactive-power coupling by augmenting it with both the damping correction loop and the transient droop function. Unlike VSGs equipped with either of these two designs alone, combining them provides more control freedom and thus results

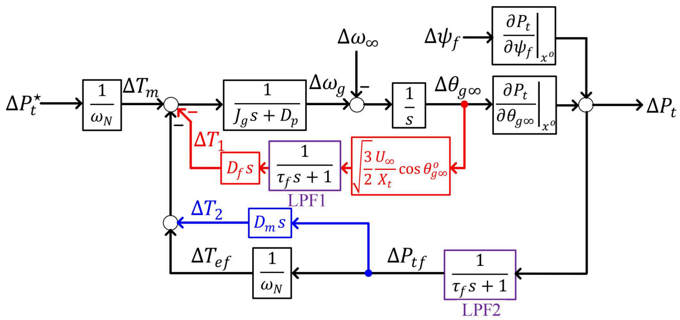

Fig. 7. Block diagram for small-signal model of the APL (including LPF1 and LPF2 marked in purple colour). Blocks marked in red are associated with the damping correction loop, and the one in blue is related to the transient droop function.

in better APL and RPL coupling reduction performance. Also, the proposed design is able to adjust the APL response speed without affecting the steady-state frequency-droop characteristics. The proposed VSG design may be widely adopted in applications related to renewable energy integration, HVDC transmission systems, and flexible AC transmission systems. Future work includes the complete decoupling of VSG APL and RPL under both the inductive and resistive grid conditions. Another compelling avenue for future work is hardware implementation of the proposed controller, which would validate its robustness against effects of non-idealities in practice, such as measurement noise and signal delay.

Appendix

A. Derivation of APL Parameter Settings in (20)–(22)

To obtain the closed-form expressions for APL parameters J_g, D_f, and D_m, we include LPF1 and LPF2 in the VSG APL model and construct the corresponding small-signal model based on Fig. 1. The block diagram of the resulting small-signal APL model is shown in Fig. 7. The corresponding transfer-function model is as follows:

$$\Delta P_t = \frac{N_1(s)\Delta P_t^\star + N_2(s)\Delta\omega_\infty + N_3(s)\Delta\psi_f}{s^3 + bs^2 + Ks + d}, \tag{23}$$

where

$$b = \frac{J_g + D_p\tau_f}{J_g\tau_f}, \qquad d = \sqrt{\frac{3}{2}}\frac{\psi_f^\circ U_\infty \cos\theta_{g\infty}^\circ}{J_g\tau_f X_t},$$
$$K = \frac{1}{\tau_f J_g}\left(D_p + \left(D_f + D_m\omega_N\psi_f^\circ\right)\sqrt{\frac{3}{2}}\frac{U_\infty\cos\theta_{g\infty}^\circ}{X_t}\right).$$

We refrain from providing expressions for $N_1(s)$, $N_2(s)$, and $N_3(s)$ for brevity. By tuning J_g, D_f, and D_m, we wish to endow (23) with two dominant poles $\lambda_{2,3}^\star = -\omega_n^\star\zeta^\star \pm j\omega_n^\star\sqrt{1-(\zeta^\star)^2}$ (which are roots of the characteristic equation of (23)), where $\omega_n^\star$ and $\zeta^\star$, respectively, denote the desired natural frequency and the damping ratio for the APL dominant mode, corresponding to desired APL dynamic behaviour. We also set β to its desired value $\beta^\star$. Further let $\lambda_1^\star = -\alpha_1 < 0$, denote the remaining unspecified real-valued root of the characteristic equation of (23). According to Vieta's theorem [19],

$$-b = s_1 + s_2 + s_3 = -\alpha_1 - 2\omega_n^\star\zeta^\star, \tag{24}$$
$$K = s_1s_2 + s_2s_3 + s_1s_3 = 2\alpha_1\omega_n^\star\zeta^\star + {\omega_n^\star}^2, \tag{25}$$
$$-d = s_1s_2s_3 = -\alpha_1{\omega_n^\star}^2. \tag{26}$$

Then, by solving J_g, D_f, and D_m from (24)–(26), we arrive at the *closed-form* expressions (20)–(22) for control parameters J_g, D_f, and D_m.

References

[1] D. Dong, B. Wen, D. Boroyevich, P. Mattavelli, and Y. Xue, "Analysis of phase-locked loop low-frequency stability in three-phase grid-connected power converters considering impedance interactions," *IEEE Trans. Ind. Electron.*, vol. 62, no. 1, pp. 310–321, Jan. 2015.

[2] H. P. Beck and R. Hesse, "Virtual synchronous machine," in *Proc. 9th Int. Conf. EPQU*, 2007, pp. 1–6.

[3] Q.-C. Zhong and G. Weiss, "Synchronverters: Inverters that mimic synchronous generators," *IEEE Trans. Ind. Electron.*, vol. 58, no. 4, pp. 1259–1267, Apr. 2011.

[4] S. Dong and Y. C. Chen, "Adjusting synchronverter dynamic response speed via damping correction loop," *IEEE Trans. Energy Convers.*, vol. 32, no. 2, pp. 608–619, Jun. 2017.

[5] S. Dong and Y. C. Chen, "A method to directly compute synchronverter parameters for desired dynamic response," *IEEE Trans. Energy Convers.*, vol. 33, no. 2, pp. 814–825, Jun. 2018.

[6] T. Shintai, Y. Miura, and T. Ise, "Oscillation damping of a distributed generator using a virtual synchronous generator," *IEEE Trans. Power Del.*, vol. 29, no. 2, pp. 668–676, Apr. 2014.

[7] Y. Li, R. Qi, and S. Wang, "New control schemes of output power decoupling based on synchronverter," in *Proc. 21th Int. Conf. Electr. Mach. Syst. (ICEMS)*, 2018, pp. 1980–1985.

[8] M. Li, Y. Wang, N. Xu, W. Wang, Y. Liu, H. Wang, and Y. Weizheng, "A power decoupling control strategy for droop controlled inverters and virtual synchronous generators," in *Proc. IEEE 8th Int. Power Electron. Motion Control Conf. (IPEMC-ECCE Asia)*, 2016, pp. 1713–1719.

[9] X. Li, Y. Hu, Y. Shao, and G. Chen, "Mechanism analysis and suppression strategies of power oscillation for virtual synchronous generator," in *43rd Annu. Conf. IEEE Ind. Electron. Soc. (IECON)*, Oct. 2017, pp. 4955–4960.

[10] Y. Liu, Y. Wang, M. Li, N. Xu, W. Wang, N. Wang, H. Wang, and J. Wu, "Improvement of reactive power dynamic response for virtual synchronous generator," in *Proc. IEEE 8th Int. Power Electron. Motion Control Conf. (IPEMC-ECCE Asia)*. IEEE, 2016, pp. 2010–2014.

[11] Q.-C. Zhong, W. L. Ming, and Y. Zeng, "Self-synchronized universal droop controller," *IEEE Access*, vol. 4, pp. 7145–7153, Oct. 2016.

[12] J. Chen and T. O'Donnell, "Parameter constraints for virtual synchronous generator considering stability," *IEEE Trans. Power Syst.*, vol. 34, no. 3, pp. 2479–2481, May 2019.

[13] S. D'Arco, J. A. Suul, and O. B. Fosso, "A virtual synchronous machine implementation for distributed control of power converters in smart grids," *Elect. Power Syst. Res.*, vol. 122, pp. 180–197, 2015.

[14] J. Fang, X. Li, and Y. Tang, "Grid-connected power converters with distributed virtual power system inertia," in *n Proc. 2017 IEEE Energy Convers. Congr. Expo.*, Oct. 2017, pp. 4267–4273.

[15] L. Huang, H. Xin, Z. Wang, K. Wu, H. Wang, J. Hu, and C. Lu, "A virtual synchronous control for voltage-source converters utilizing dynamics of dc-link capacitor to realize self-synchronization," *IEEE J. Emerg. Sel. Topics Power Electron.*, vol. 5, no. 4, pp. 1565–1577, Dec. 2017.

[16] J. M. Guerrero, L. G. de Vicuna, J. Matas, M. Castilla, and J. Miret, "A wireless controller to enhance dynamic performance of parallel inverters in distributed generation systems," *IEEE Trans. Power Electron.*, vol. 19, no. 5, pp. 1205–1213, Sep. 2004.

[17] Y. Li and Y. W. Li, "Power management of inverter interfaced autonomous microgrid based on virtual frequency-voltage frame," *IEEE Trans. Smart Grid*, vol. 2, no. 1, pp. 30–40, Mar. 2011.

[18] P. Zhang, H. Zhao, H. Cai, J. Shi, and X. He, "Power decoupling strategy based on virtual negative resistor for inverters in low-voltage microgrids," *IET Power Electron.*, vol. 9, no. 5, pp. 1037–1044, Apr. 2016.

[19] J. W. Harris and H. Stöcker, *Handbook of Mathematics and Computational Science*. New York: Springer-Verlag, 1998.